SCHELLENG IN RETROSPECT – A SYSTEMATIC STUDY OF BOW FORCE LIMITS FOR BOWED VIOLIN STRINGS

Erwin Schoonderwaldt,[1] Knut Guettler,[2] Anders Askenfelt[1]
*[1] Dept. of Speech, Music and Hearing, Royal Institute of Technology (KTH),
SE-10044 Stockholm, Sweden, {schoondw, andersa}@speech.kth.se
[2] Norwegian Academy of Music, P.O. Box 5190 Majorstuen, Oslo 0302, Norway,
knut.guettler@nmh.no*

Abstract

An experimental study of the upper and lower bow force limits for bowed violin strings is reported. A bowing machine was used to perform bow strokes with a real violin bow on steel D and E strings mounted on a rigid monochord and on a violin, respectively. Measurements were systematically performed for 24 values of bow force and 11 values of relative bow-bridge distance at four bow velocities (5, 10, 15 and 20 cm/s). The measured string velocity signals were used to compile Schelleng diagrams, showing the distribution of different classes of string motion (multiple slipping, Helmholtz motion, raucous motion). It was found that the maximum bow force limit for Helmholtz motion corresponded well to Schelleng's equation in modified form, taking the shape of the (hyperbolic) friction curve into account. The minimum bow force was found to be independent of bow velocity, which is in clear contradiction to Schelleng's prediction. Observations and simulations suggested that the breakdown of Helmholtz motion at low bow forces involves a mechanism related to ripple and corner rounding which was not taken into account in Schelleng's derivation of minimum bow force.

INTRODUCTION

In playing a bowed string instrument the sound is mainly controlled by the three main bowing parameters bow velocity (v_B), bow force (F_B), and relative bow-bridge distance (β). The production of a good tone characterized by Helmholtz motion requires a precise coordination of these bowing parameters. Schelleng [1973] formalized the maximum and minimum bow force for production of Helmholtz motion, given v_B and β:

$$F_{\min} = \frac{Z_0^2 v_B}{2R(\mu_s - \mu_d)\beta^2} \quad , \tag{1}$$

$$F_{\max} = \frac{2Z_0 v_B}{(\mu_s - \mu_d)\beta} \quad , \tag{2}$$

with Z_0 the characteristic impedance of the string, R the mechanical damping, μ_s the static friction coefficient and μ_d the dynamic friction coefficient at the bow-string contact. In a log-log representation of relative bow force versus relative bow-bridge distance known as the Schelleng diagram the upper and the lower bow force limit form straight lines with slopes of -1 and -2, respectively, under the assumption that the friction coefficient delta ($\mu_s - \mu_d$) is constant.

The latter assumption is not generally valid, especially not at small values of v_B and large values of β. The Schelleng equations (1) and (2) can be modified taking the

functional form of the friction curve into account. This was shown by Schelleng [1973] for the minimum bow force for a hyperbolic friction curve of the form:

$$\mu = \mu'_d + K/(z - z_0) \quad , \tag{3}$$

with z the relative slip velocity v_B/β, z_0 a translational constant for obtaining a finite value of μ_s, μ_d' the asymptote for $z \to \infty$ and K a constant determining the curvature of the friction curve. Using Eq. (3) ($\mu_s - \mu_d$) can be expressed as function of v_B and β, which by substitution into Eqs. (1) and (2) yields the modified Schelleng equations:

$$F_{min} = \frac{Z_0^2}{2R(\mu_s - \mu'_d)} \cdot \frac{v_B + \beta z_0}{\beta^2} \quad , \tag{4}$$

$$F_{max} = \frac{2Z_0}{(\mu_s - \mu'_d)} \cdot \frac{v_B + \beta z_0}{\beta} \quad . \tag{5}$$

In the modified form the Schelleng equations account for the finite minimum bow force when v_B approaches zero, as observed in experiments (e.g., [Raman, 1920]). Furthermore, the bow force limits in the Schelleng diagram are curved according to Eqs. (4) and (5), especially at small values of v_B in which case the term βz_0 gains relative importance.

Only a few experimental studies of the bow-force limits have been published, most of them focusing on the minimum bow force, e.g., Raman [1920], Lazarus (see [Cremer, 1984]). Also bowed-string simulations have been done investigating the relationship between minimum bow force and the resonance properties of the instrument [Woodhouse, 1993]. Schumacher [1994] measured the maximum bow force for a number of different strings. The results suggested a good agreement between the observed maximum bow force and Schelleng's equation in a generalized form (cf. Eq. (5)) taking rotational compliance of the string into account.

Previous experimental verifications of a complete Schelleng diagram have been limited to a cello D string at a single bow velocity [Galluzzo, 2003]. The bow used was a rosined Perspex rod for better comparison with bowed-string simulations. Also this study indicated that the observed bow-force limits were in accordance with Schelleng's equations.

The aim of the current study is to perform a systematic experimental investigation of the bow-force limits using a real violin string and a real bow. The observed behaviour will be compared to the predictions of Schelleng's equations in order to provide an empirical evaluation of the latter. The results might give a better insight in the bow-force limits as experienced by the player and provide new reference material for bowed-string simulations.

METHOD

Empirical Schelleng diagrams were obtained for violin D and E strings mounted on a monochord using a normal violin bow. The bow was driven by a computer-controlled bowing machine [Cronhjort, 1992], enabling accurate control of bow velocity and bow force. The ranges of β, v_B and F_B were chosen to represent a substantial part of the control space in normal violin playing (see e.g. [Askenfelt, 1989]). The β range (about 1/30-1/6) was divided into a grid of 11 logarithmically spaced values and the F_B range (49-3000 mN) was divided into a grid of 24 logarithmically spaced values, forming the "pixels" of the Schelleng diagram. Schelleng diagrams were measured at four different bow velocities of 5, 10, 15 and 20 cm/s.

The strings used were a Prim D string (medium) with a steel core and a chrome steel winding and a Prim E string (medium) of plain steel. The bow was a carbon fiber composite bow manufactured by Leopold. The width of the bow hair ribbon was 10 mm. The monochord was a stiff duraluminium bar with U-shaped cross section glued onto a solid piece of hardwood. The effective string length was 325 mm. At both string supports a piece of tape was applied to improve the string-support contact and add appropriate damping. Without the tape it was observed that pizzicato notes could result in sitar-like sounds indicating the presence of a nonlinear interaction between the string and the support.

The following procedure was used for measuring Schelleng diagrams. First the bow-bridge distance was set by aligning the bowing machine relative to the violin. The bow was always flat on the string (no tilting) and the middle of the bow hair ribbon was taken as the reference point for setting the bow-bridge distance. The estimated accuracy of the bow-bridge distance was about 0.5 mm. Then a sequence of bow strokes was performed with incrementing bow force and three repetitions at each bow force. The velocity and force contours of the bow strokes were designed so that Helmholtz motion was obtained during the attack phase after which the bow force was smoothly changed to its target value. The steady part of bowing lasted 0.5-4 s depending on the bow velocity (limited by the maximum range of 30 cm allowed for by the bowing machine). This was done for the 11 different values of β in random order to avoid possible trends, for example due to the wearing out of the rosin. A new layer of rosin was applied before each measurement session, good for about half a Schelleng diagram.

For the classification of the string motion the string velocity signal was used, which was obtained by placing a small magnet (diameter 6 mm) under the string at the bowing point and measuring the induced voltage. The signal was amplified using a Symmetrix SX 202 balanced microphone pre-amplifier and recorded using a Tascam US-122 external sound device at a sampling rate of 44.1 kHz.

A novel interactive method was developed for the classification of the string motion, consisting of the following steps. First, a selection was made of about 10 fundamental periods well within the steady part of bowing. Second, the slip phases were detected using a simple velocity threshold criterion. The default threshold value was $-v_B$,[1] but could be changed by the experimenter after visual inspection. Third, for each detected slip phase the slip-to-slip time interval was calculated (using linear interpolation to find the zero-crossings) as well as the string displacement under the bow. These features were displayed in a scatter plot of displacement vs. time, further referred to as a classification diagram.

The classification diagrams reveal clear differences between different types of string motion. In case of Helmholtz motion all slip phases coincide at one point corresponding to the fundamental period T_0 at the time axis and the extent of the string displacement at the bowing point $(1-\beta)T_0 v_B$ at the displacement axis. In case of multiple slipping motion clusters are formed for the different slip phases within one fundamental period, indicating the persistence of this type of motion. In case of raucous motion the slip phases are randomly distributed across the classification diagram also at higher values than T_0 and the nominal displacement extent, indicating aperiodicity and the presence of prolonged stick phases.

---

[1] As the string velocity signal was not calibrated the value of v_B was estimated by taking the median of the stick phases.

RESULTS

Empirical Schelleng diagrams of the D string

The Schelleng diagrams obtained for the violin D string are shown in Fig. 1. The different types of string motion are indicated with different symbols. At all bow velocities a continuous region of Helmholtz motion could be observed with clear upper and lower bow force limits. The triangular shape of the Helmholtz region was roughly in agreement with Schelleng's predictions, as can be seen from the fitted bow force limits according to eqs. (1) and (2), indicated with solid lines in Fig. 1. Below the lower bow-force limit mostly multiple slipping motion was observed. Above the upper bow force limit there was mostly raucous motion, but also cases of anomalous low frequency [Guettler, 1994] and possibly S-motion [Lawergren, 1983].

The four different panels in Fig. 1 show that there was a clear dependence of the playable region on bow velocity. The upper bow-force limit showed a clear upward shift with increasing bow velocity. On the other hand, the lower bow-force limit was rather constant. This will be discussed in more detail below.
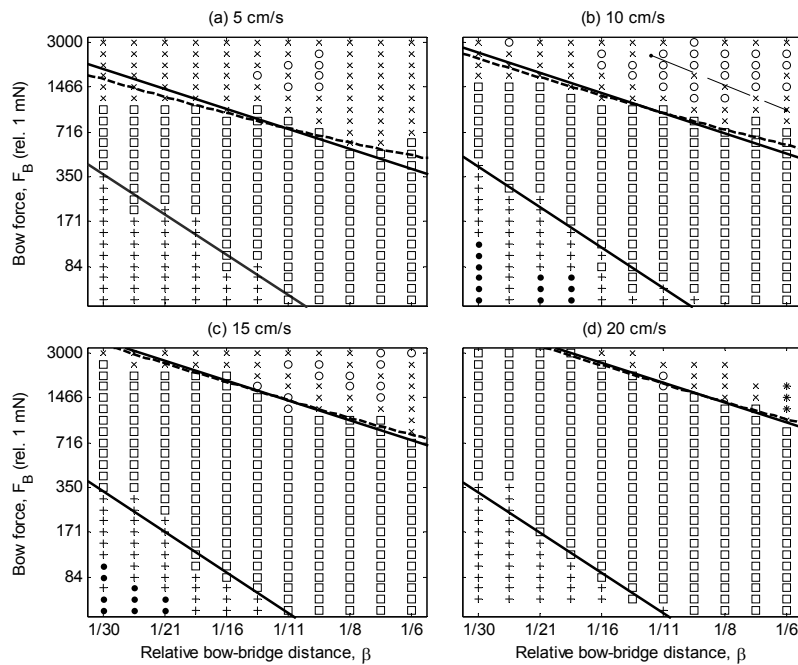
Fig. 1: Empirical Schelleng diagrams for a violin D string mounted on a monochord at four bow velocities. The symbols indicated the type of string motion: Helmholtz (□), multiple slipping (+), constant slipping (•), raucous (×), anomalous low frequencies (o), and S-motion (*). The solid lines indicate the fitted bow force limits according to eq. (1) and (2). The dashed lines indicated the fitted upper bow force limit using eq. (5).

Fitting of Schelleng's equations

According to eqs. (1) and (2) the lower and the upper bow force limits are proportional to $1/\beta^2$ and $1/\beta$, respectively, at constant bow velocity, under the assumption that $(\mu_s - \mu_d)$ is constant. In the Schelleng diagram the bow force limits are represented by straight lines with slopes -2 and -1, respectively. The constants of proportionality c_{lower} ($Z_0^2 v_B / 2R(\mu_s - \mu_d)$) and c_{upper} ($2Z_0 v_B / (\mu_s - \mu_d)$) defining the bow-force limits could be evaluated by fitting eqs. (1) and (2) to the observed bow-force limits. The fitting was performed in the logarithmic domain using a least-squares method.

The resulting Schelleng limits are indicated in Fig. 1 with the solid lines. The Schelleng limits showed a good agreement with the observed limits for higher v_B. However, for lower values of v_B substantial deviations of the slope were observed for the upper bow-force limits, the observed slopes being less steep than the predicted slope of -1.

Alternatively, the modified Schelleng equations (4) and (5) were fitted to the observed bow-force limits, taking into account a functional (hyperbolic) dependence of the friction curve on v_B and β rather than assuming that $(\mu_s - \mu_d)$ is constant. The resulting fits for the upper bow-force limits are indicated in Fig. 1 with the dashed lines. It can be seen that the modified Schelleng equation provided a better fit to the data, the slopes becoming less steep with decreasing v_B.

Empirical Schelleng diagrams of the E string

As the properties of the strings of the violin vary greatly from the G to the E string, the bow force limits are expected to show differences as well. In order to investigate this, empirical Schelleng diagrams were obtained for the E string at bow velocities of 10 and 20 cm/s (see Fig. 2). The fitted bow-force limits according to eqs. (1) and (2) are indicated with the solid lines. For comparison, the fitted bow-force limits of the D string are indicated with dotted lines. At $v_B = 10$ cm/s the upper bow force limit of the E string was found to be 19% lower, while the lower bow force limit was 64% lower. The playable region of the E string is relatively large compared to the D string. This is most likely due to the lower internal losses in the solid E string compared to the wound D string, causing a decrease of the minimum bow force [Schoonderwaldt et al., 2007].
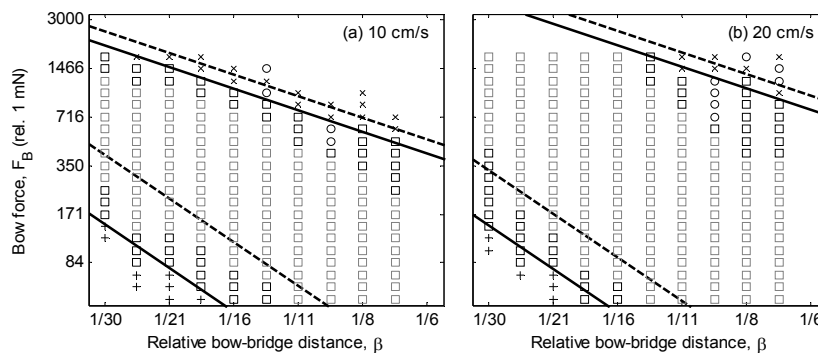
Fig. 2: Empirical Schelleng diagrams for a steel E string mounted on a monochord at two bow velocities. The fitted bow force limits according eq. (1) and (2) are indicted with solid lines. For comparison the fitted bow force limits of the D string are indicated with dashed lines.

Dependence of bow-force limits on bow velocity

According to eqs. (1) and (2) the minimum and maximum bow-force limits should be proportional with bow velocity. As already mentioned the upper bow-force limits showed a clear upward shift for increasing bow velocity, but the lower bow-force limit remained constant. The dependence of \cupper and \clower on v_B is shown in Fig. 3. The maximum bow force (panel (a)) was clearly proportional to bow velocity, as can be seen from the fitted line (forced to go through the origin). Only at $v_B = 5$ cm/s the maximum bow force showed a marked deviation from this trend. In contrast, the minimum bow force showed no clear dependence on bow velocity as can be seen in panel (b). The dependence of the bow force limits on bow velocity was the same for both the D and the E string.
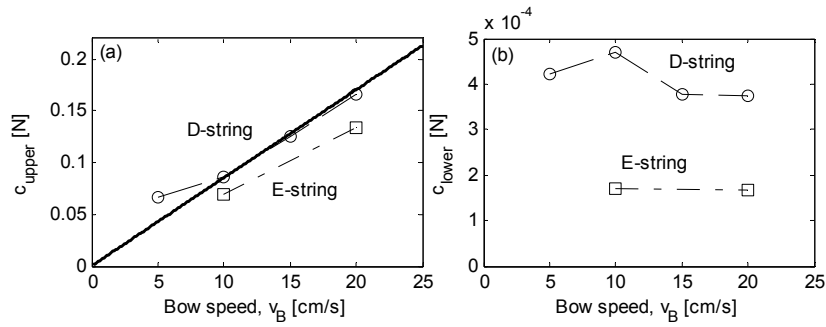
Fig. 3: Dependence of the bow-force limits on bow velocity. The plots show the fitted values of c_{upper} (a) and c_{lower} (b) for both the D string (o) and the E string (□).

Breakdown of Helmholtz motion at minimum bow force

More insight in the breakdown of Helmholtz motion at minimum bow force was gained by using bow strokes with gradually decreasing bow force. The initial force and the force gradient were chosen so that the string was in Helmholtz motion in the beginning of the decreasing phase and the minimum bow force was reached in about the middle of that phase. A typical transition from Helmholtz to multiple slipping motion is shown in Fig. 4. In panel (a) it can be clearly seen from the envelope that the string motion becomes unstable after the transition (indicated with the dashed line).

The other panels show extracted features of the slip phase, namely maximum string velocity reached during the slip phase $v_{S, max}$ (panel (b)), the slip duration T_{slip} and the time interval of the slip phase measured at half-height of the slip phase $T_{slip, half-height}$ (panel (c)). The latter should correspond to the nominal duration of the slip phase for ideal Helmholtz motion βT_0, where T_0 the fundamental period of vibration, which is indicated with the dashed horizontal line in panel (c). Each point in panel (b) and (c) corresponds to one detected slip phase.
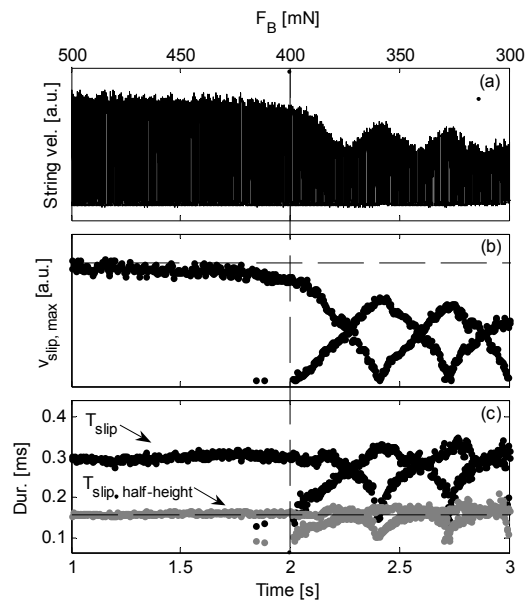
Fig. 4: Breakdown of Helmholtz motion at minimum bow force (D string). Shown are (a) The string velocity signal, (b) the maximum slip velocity for each detected slip phase, and (c) the slip duration at the zero-crossing (T_{slip}) and at half-height of the slip phase ($T_{slip\ half-height}$).

Panel (b) and (c) show clearly the evolution of the shape of the slip phase as the bow force decreases. Before the transition it can be seen that $v_{S,\,max}$ decreased to below the nominal slip velocity for ideal Helmholtz motion (indicated with the dashed horizontal line in panel (b) by the dashed horizontal line). Simultaneously, T_{slip} showed an increase. This change of the shape of the slip phase can be attributed to corner rounding, which becomes more pronounced with decreasing bow force. At the transition, it can be seen that a second slip phase started to develop. At about $t \approx 2.3$ s it can be seen that the second slip phase became dominant over the former main slip, which finally disappeared completely. After the transition new slip phases were formed and disappeared, leading to a sort of permanent state of transient behaviour.

Breakdown of Helmholtz motion in bowed string simulations

As already mentioned in the introduction Schelleng's minimum bow force is based on Raman's string model. It is however well known that this model is not very realistic. The reflection functions of this model are of the dirac-delta type. As can be seen in Fig. 5 (a) the friction force is rising in steps from a minimum value equal to $F_B\mu_d$ during the slip phase to a maximum close to the middle of the stick phase (when the string is bowed at an integer-ratio position). However, with any kind of more realistic damping, the step-like force build-up would be replaced by a force ripple, with maxima most likely to occur at the instance βT_0 before the stick-slip transition (caused by reflections from the nut), or βT_0 after the slip-stick transition (caused by reflections from the bridge). This force ripple is the result ('echo') of rounded-corner sharpening at the bowing point, a feature not present in Raman's model. Simulations show that the ripple amplitudes are dependent on the length of the slip interval, friction-coefficient delta, and damping properties, but are not proportional to bow velocity.

Fig. 5 shows the effect of Raman damping versus a moving-average type of damping. In both cases the minimum bow force is determined by the range of periodic friction-force variation, equal to $F_B(\mu_s - \mu_d)$, as indicated in Fig. 5 for the different cases by the double arrows. As opposed to the Raman model (panel (a)), which shows a proportional relation between minimum bow force and bow velocity, the model with narrow reflection functions shows a mere 17% increase of minimum bow force when bow velocity is increased from 5 to 20 cm/s. More generally, simulations showed that the influence of bow velocity on minimum bow force is strongly reduced for large values of β, and shows only limited effects (always less than proportional) at smaller values of β.
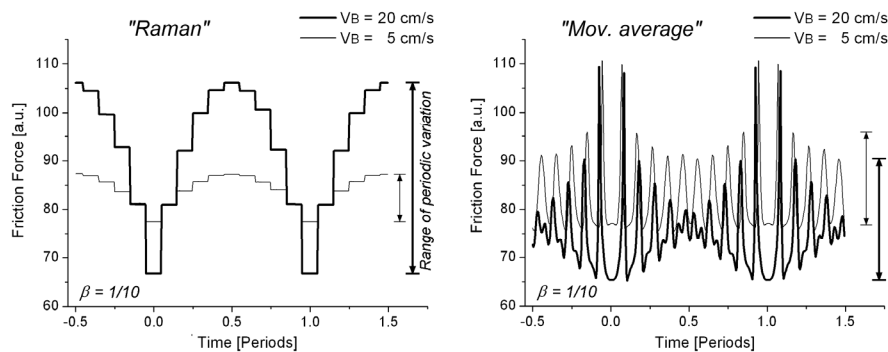
Fig. 5: Periodically repeating patterns of friction force simulated with a hyperbolic friction model using (a) Raman's string model, and (b) a model with narrow reflection functions.

CONCLUSIONS

Generally, the empirical Schelleng diagrams showed good qualitative agreement with the predictions of Schelleng. A well-defined playable region with Helmholtz motion was found. Both the upper and the lower bow-force limits decreased with increasing β, the lower limit more strongly than the upper limit.

Closer inspection of the upper bow-force limit revealed that the slope of the observed limit was less steep than the predicted Schelleng slope of -1, especially at low bow velocities. This could be attributed to a decrease of the friction-coefficient delta for decreasing bow velocities, which was shown by fitting a modified version of Schelleng's equation taking the functional shape of the (hyperbolic) friction curve into account.

The measurements indicated that the minimum bow force was independent of bow velocity in the range of 5 to 20 cm/s. This was confirmed by simulations comparing Raman's string model on which Schelleng's minimum bow force is based with a more realistic model with narrow reflection functions. The simulations showed that the minimum bow force increased only with 17% when increasing the bow velocity from 5 to 20 cm/s, instead of a 300% increase for the Raman model. The reason for this discrepancy is the role of friction-force ripple resulting from corner sharpening at the bowing point, which is ignored in Raman's model.

ACKNOWLEDGEMENTS

REFERENCES

Askenfelt, A. (**1989**), "Measurement of the bowing parameters in violin playing. II: Bow-bridge distance, dynamic range, and limits of bow force." *J. Acoust. Soc. Am.* 86 (2), pp 503-516.

Cremer, L. (**1984**), *The physics of the violin*, The MIT Press.

Cronhjort, A. (1992), "A computer-controlled bowing machine (mums)," *STL-QPSR* 33 (2-3) pp. 61-66.

Galluzzo, P.M. (**2003**), *On the playability of stringed instruments*, PhD dissertation, Trinity College, University of Cambridge.

Guettler, K. (**1994**), "Wave analysis of a string bowed to anomalous low frequencies," *Catgut Acoust. Soc. J.* 2 (6), pp. 8-14.

Lawergren, B. (**1983**), "Harmonics of s motion on bowed strings," *J. Acoust. Soc. Am.* 73 (6), pp. 2174-2179.

Raman, C.V. (**1920**), "Experiments with mechanically-played violins," In Proc. *Indian Assoc. Cultivation Sci.* Vol. 6, pp. 19-36.

Schelleng, J.C. (**1973**), "The bowed string and the player," *J. Acoust. Soc. Am.* 53 (1) pp. 26-41.

Schoonderwaldt, E.; Guettler, K.; Askenfelt, A. (**2007**), "An empirical investigation of bow-force limits in the Schelleng diagram," *Manuscript submitted for publication.*

Schumacher, R.T. (**1994**), Measurement of some parameters of bowing. *J. Acoust. Soc. Am.* 96 (4) pp. 1985-1998.

Woodhouse, J. (**1993**), "On the playability of violins. part II: Minimum bow force and transients," *Acustica*, 78, pp. 137-153.